Research Article

Chaitanya Mayee Makkuva* and Vijaya Babu Vommi

Mechanical improvement in acetal composites reinforced with graphene nanotubes and Teflon fibers using loss functions

https://doi.org/10.1515/jmbm-2024-0032
received July 03, 2024; accepted January 03, 2025

Abstract: This study focuses on improving the mechanical strength, wear resistance, and frictional properties of acetal, a popular engineering polymer, by incorporating graphene nanotubes (GNTs) and Teflon fibers. Despite acetal's low friction and chemical resistance, its mechanical limitations often restrict its use in high-load, wear-intensive applications. To overcome this, researchers developed composite materials using a melt-blending technique with varying concentrations of GNTs (0.25–2.0 wt%) and Teflon fibers (5–20 wt%). Key findings include a significant enhancement in acetal's mechanical properties with the addition of 1 wt% silane-treated GNTs, resulting in increases of 34% in tensile strength, 48% in tensile modulus, 44% in flexural strength, and 47% in flexural modulus compared to pure acetal. Furthermore, incorporating 10 wt% Teflon fibers reduced wear rates by 58% and improved frictional performance. The optimized composite, containing 1 wt% GNTs and 10 wt% Teflon fibers, demonstrated superior mechanical and tribological properties, making it suitable for demanding engineering applications such as gears. This research underscores the potential of acetal composites for enhancing performance and durability in mechanical components, paving the way for more efficient and sustainable engineering solutions while advancing polymer composite material development.

Keywords: multiple attribute decision making, loss functions, acetal copolymer, graphene nano tubes, polymer gears, Teflon fiber, and best alternative

*** Corresponding author: Chaitanya Mayee Makkuva**, Department of Mechanical Engineering, Andhra University, Visakhapatnam, 530003, AP, India, e-mail: mayee.chaitu@gmail.com
Vijaya Babu Vommi: Department of Mechanical Engineering, Andhra University, Visakhapatnam, 530003, AP, India

1 Introduction

Polymer gears are widely utilized in industries such as food processing, automotive, aerospace, and biomedical sectors, due to their notable characteristics, including silent operation, self-lubricating properties, and cost-effectiveness [1]. Among the various polymer materials, acetal stands out as a preferred choice for gear production. This preference stems from its unique properties, such as a low coefficient of friction, high resistance to abrasion, wear, and fatigue, and exceptional dimensional stability. However, the performance and load-bearing capacity of acetal gears are significantly influenced by the material's stiffness, fatigue resistance, and wear-resistant attributes [2]. To broaden the application scope of acetal gears, these properties need improvement.

Enhancing stiffness and fatigue resistance can mitigate internal heat generated due to the hysteresis effect. Similarly, improving wear resistance reduces the high temperatures that occur at the contact points of meshing gear teeth, thereby increasing the gears' load-bearing capacity and overall lifespan [3]. Recent advancements have seen researchers focus on extending the life and enhancing the performance of polymer gears by incorporating lubricating additives (*e.g.*, PTFE, oils, and grease) and reinforcements [4] (*e.g.*, glass fibers, carbon fibers).

A promising research direction involves the use of graphene nanotubes (GNTs) as reinforcements to improve the mechanical and tribological properties of polymer composites. However, effective dispersion of GNTs within the polymer matrix is a significant challenge due to their high aspect ratio, tendency for agglomeration, and strong van der Waals forces. Proper dispersion is critical as it increases the surface area available for interaction with the matrix, reducing stress concentrations [5,6]. Furthermore, achieving a strong interfacial bond between GNTs and the polymer matrix is essential for efficient load transfer, which directly impacts the mechanical performance of the composite. Due to GNTs' inert nature, they

often form weak bonds with the matrix, necessitating surface modifications through techniques such as carboxylation, silanation, carbonylation, and amination.

Studies on functionalized GNT-reinforced acetal composites are limited, especially regarding how various GNT functionalizations influence wear resistance and lifespan. Exploring these effects is critical for developing composites with superior performance [7]. For acetal gears, enhancing not only the mechanical properties but also the frictional and wear characteristics is crucial for extending their operational life and broadening their application range.

In efforts to achieve these enhancements, researchers have incorporated lubricating additives like Teflon and graphene into acetal composites. Among these, Teflon is particularly noteworthy for its low friction coefficient, although its softness limits its wear resistance [8]. However, when combined with other materials, Teflon contributes significantly to wear resistance by forming a lubricating film on gear surfaces.

To advance the development of acetal gears, a novel approach involves creating acetal/GNT-reinforced Teflon composites using melt compounding with a twin-screw extruder. The GNTs are functionalized using the aforementioned techniques to improve dispersion and interfacial bonding with the acetal matrix. Spectral analysis is employed to confirm these surface modifications, and the resulting composites are evaluated for their tensile, flexural, and wear properties. This approach aims to enhance the mechanical performance, wear resistance, and lifespan of acetal gears, ultimately expanding their practical applications [9,10].

2 Experimental details

2.1 Materials

Acetal copolymer, which stands as the prevailing choice among engineering thermoplastics for applications involving gear and machinery components, serves as the foundational material. The granular form of acetal copolymer, commonly recognized as Kocetal K 700 and provided by Kolon Engineering Plastics, USA, is the selected material [11,12]. Physical and thermal properties are presented in Table 1.

GNT used for strengthening acetal is provided by Sky spring Nano Inc., USA. GNTs are produced from natural gas using catalytic chemical vapor deposition method. As seen from the transmission electron microscopy (TEM) image (Figure 1) of GNTs, the outer diameter of GNTs varies between 20 and 30 μm.

TEM is used for analyzing the dispersion of GNTs within the acetal matrix. It provides high-resolution imaging to clearly observe the GNT dimensions, ensuring uniform dispersion and identifying any agglomeration, which is critical for enhancing composite properties.

Table 1: Physical and thermal properties of acetal copolymer

Property	Value
Melt flow index	27 g/10 min
Specific gravity	1.41
Melting point	166°C
Heat deflection temperature (0.45 MPa)	158°C
Vicat softening temperature	160°C
Coefficient of thermal expansion	13×10^{-5} cm/cm °C

2.2 Methodology

2.2.1 Functionalization of GNTs

Functionalizaton of GNTs involves a comprehensive array of techniques, encompassing carboxylation, silanation, carbonylation, and amination, to attain a uniform dispersion of GNTs throughout the matrix, thereby enhancing compatibility. These actions are further elucidated in the subsequent sections, delineating the meticulous considerations for these surface modifications.

2.2.2 Purification process of GNTs

GNTs are carried out with great precision, involving a series of steps to eliminate amorphous carbon and other impurities initially. To ensure the removal of volatile vapors and contaminants, the GNTs underwent a critical

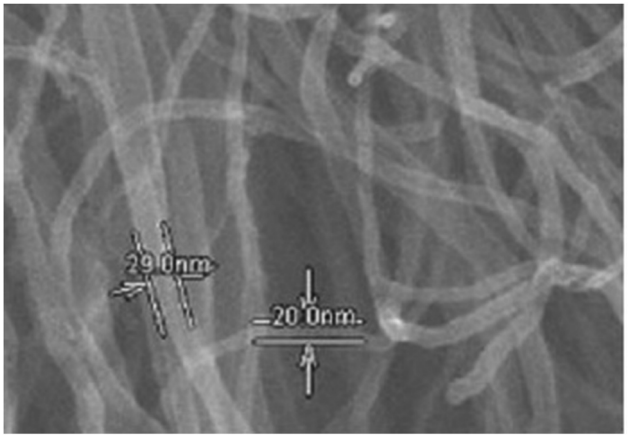

Figure 1: TEM image of the composite.

calcination process at a temperature of 500°C for a duration of 45 min upon their receipt. Following this calcination step, the resulting calcined GNTs were carefully dissolved in distilled water, combined with concentrated hydrochloric acid in a 1:1 ratio by volume, and subjected to agitation for a period of 5 h, employing a magnetic stirrer. Subsequently, the suspension was allowed to settle for a span of 24 h, during which time, the unwanted contaminants naturally separated and were subsequently removed. To further refine the product, the suspension was meticulously cleansed with distilled water. The final step in the purification process involved vacuum filtration, utilizing a 0.22 μm Teflon membrane, until the desired pH level of 7 was achieved. Finally, the filtered solid was gently dried within a vacuum oven, resulting in the transformation of the material into its purified form, now recognized as R-GNTs. This comprehensive purification procedure ensured the attainment of high-quality GNTs, free from impurities, volatile substances, and contaminants, ready for subsequent applications and research endeavors.

2.2.3 Carboxylation

The process involved the utilization of a concentrated mixture of sulfuric and nitric acids in a 3:1 volume ratio to oxidize the R-GNTs. The R-GNTs underwent reflux for a duration of 8 hours at a temperature of 90°C while immersed in a solution comprising three parts of sulfuric acid and one part of nitric acid (H_2SO_4:HNO_3). Subsequently, the resultant solution underwent dilution with distilled water, followed by periodic vacuum filtration cycles, until the suspension achieved a neutral pH value of 7. This pH adjustment occurred after the suspension had undergone an additional 8 h refluxing process. The sample was then subjected to drying for a period of 12 h at a temperature of 60°C within a vacuum oven. Following this, the solid masses that had formed during the drying phase were meticulously reduced to a fine powder through the use of a mortar and pestle. Henceforth, the GNTs that had undergone this acid treatment process are referred to as C-GNTs.

2.2.4 Silanation

In this phase of the process, we engaged in the silanization of GNTs by combining GNTs with silane modification and acid-treated GNTs, denoted as C-GNTs. This amalgamation was carried out in a solution consisting of a 95:5 volume ratio of ethanol to water, to which 2% amino-propyl-trimethoxy silane was added. Subsequently, the mixture

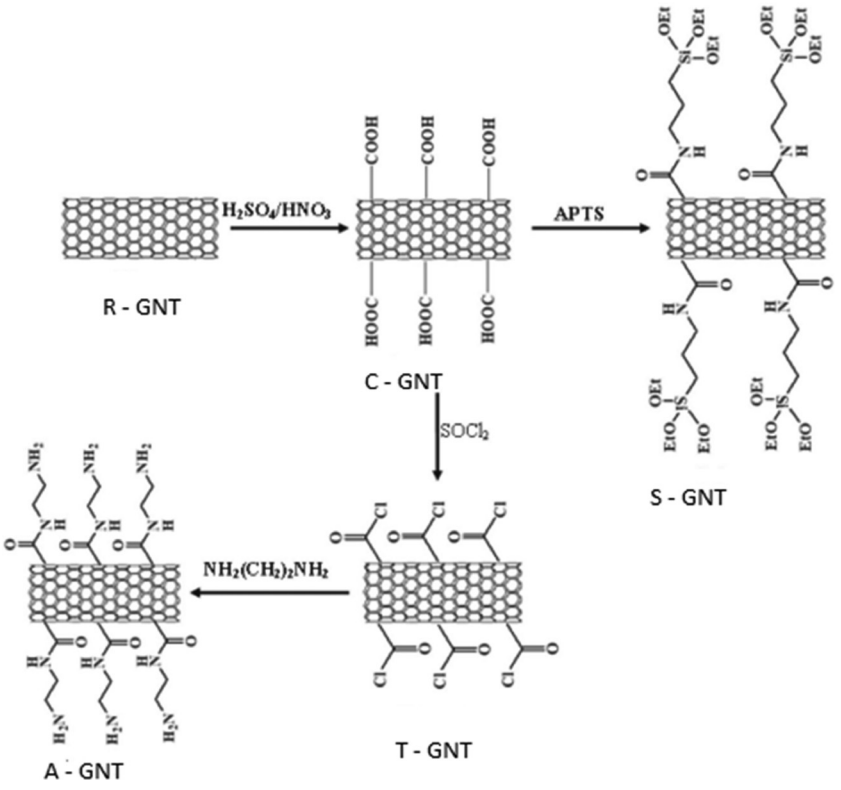

Figure 2: Schematic representation of functionalization of GNTs.

underwent an ultrasonic aging process while being stirred for a duration of 4 h. The outcome of this process was the generation of silanized GNTs, which were subsequently separated through vacuum filtration. Following this separation, the silanized GNTs underwent a thorough cleaning procedure involving acetone and water, culminating in their drying for a period of 12 h within a vacuum oven set at 60°C. These meticulously prepared GNTs are henceforth referred to as S-GNTs.

2.2.5 Carbonylation

In this particular phase of the procedure, we exclusively employed C-GNTs. The process involved suspending these C-GNTs in thionyl chloride ($SOCl_2$) prior to subjecting them to refluxing at a temperature of 65°C for a duration of 24 h. The resulting suspension was subsequently subjected to vacuum filtration through a 0.22 µm Millipore Teflon membrane and subsequently dried within a vacuum oven for 12 h at 60°C. The GNTs that emerged from this process will be denoted as T-GNTs.

2.2.6 Amination

In this phase, T-GNTs played a pivotal role as they were subjected to amination by being refluxed at 60°C for a duration of 24 h while being suspended in ethylene diamine (EDA). Following this amination process, the suspension underwent a similar drying procedure within a vacuum oven for 12 h at 60°C, coupled with vacuum filtration through a 0.22 µm Millipore Teflon membrane. Henceforth, these aminated GNTs are to be referred to as A-GNTs. A schematic representation of the GNT functionalization process is thoughtfully illustrated in Figure 2.

2.2.7 Preparation of acetal/Teflon fiber composites

To explore the impact of functionalization as well as the weight fractions of functionalized GNTs on the wear and fatigue characteristics of acetal-GNT nanocomposites, we embarked on the development of said nanocomposites. This study involved the formulation of acetal-GNT nanocomposites with varying weight fractions of functionalized GNTs. Top of Form Prior to the preparation of acetal-GNT nanocomposites through the process of melt compounding and injection molding, it is essential to subject both the acetal polymer and the GNTs to a thorough drying process within a vacuum oven set at 60°C for a duration of 12 h. This meticulous step is undertaken to eliminate any trace of moisture that may be present in the materials. The nanocomposites are then formulated with a specific

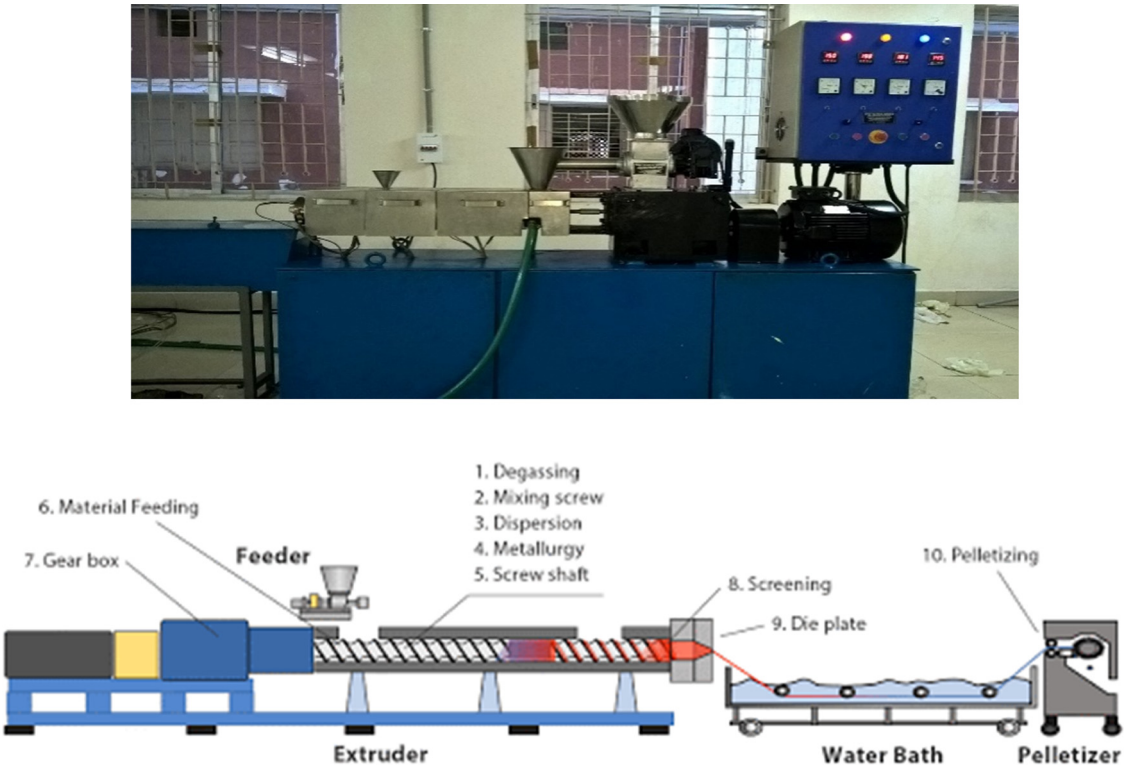

Figure 3: Twin screw extruder.

composition, consisting of 0.5 wt% of functionalized GNTs. Additionally, various weight fractions of silanized GNTs, namely, 0.25, 0.5, 1, and 2%, are incorporated into the composite matrix [13,14]. This variation in the weight fraction of silanized GNTs allows for the exploration of different material properties and performance characteristics. The actual blending of the acetal polymer and the GNTs is executed prior to the melt compounding process. This blending process involves the meticulous mixing of the requisite quantities of acetal and GNTs in a high-speed mixer. Subsequently, the blended materials are introduced into the DTS 25 twin-screw extruder, as illustrated in Figure 3. The extruder is equipped with a barrel having a diameter of 25 mm and an L/D (length-to-diameter) ratio of 32. In summary, this well-defined procedure ensures the thorough preparation of acetal-GNT nanocomposites with precise compositions, enabling the evaluation of their performance and properties in various applications [12]. The mixture is subsequently introduced at the extruder's throat. The temperature along the barrel is precisely controlled within the range of 180–190°C, while the screw's rotational speed is carefully set at 100 rpm. The resulting extrudate emerges in the form of a cylindrical wire, and it undergoes a cooling process within a water bath before being meticulously cut into pellets using a specialized pelletizer [11,15].

The various compositions of the acetal, graphene, and Teflon fiber components are reinforced with uniform dispersion and formed as thin filament using twin screw extruder. The formed filaments or wires are subjected to water bath and then subjected to pelletizing for converting them to small pieces.

Following melt compounding, all the samples underwent a meticulous drying process within a vacuum oven set at a temperature of 60°C, lasting nearly 12 h. This preparatory step was essential before proceeding to injection molding. To facilitate this, a custom injection mold, as depicted in Figure 4, was thoughtfully designed and fabricated. This mold was purpose-built for shaping both dumbbell and flat specimens, which were imperative for a diverse range of mechanical and wear tests. To execute the molding process, an advanced fully automatic vertical screw-type injection molding machine, illustrated in Figure 5, was employed. The molding conditions were meticulously calibrated, with a molding pressure of 125 MPa and a temperature of 180°C being the chosen parameters. This ensured the precise formation of the desired specimens. A fill time of 5 s, followed by a cooling period of 20 s, was strictly adhered to during the injection molding process. These settings were meticulously controlled to guarantee the consistency and quality of the resulting specimens, as showcased in Figure 6, which encompassed both tensile and flexural test specimens.

Figure 5: Vertical screw type injection molding machine.

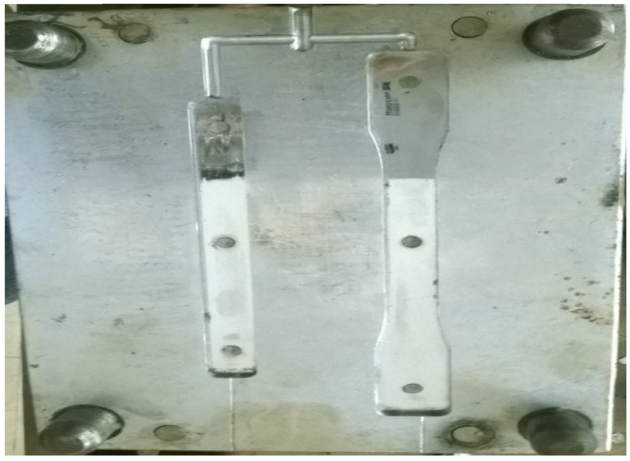

Figure 4: Test specimen's mold.

Figure 6: Injection molded test specimens.

The specimen samples were fabricated as per the ASTM D 638-08 and ASTM D 790 with the help of INSTRON 8801 mold.

The pelletized small pieces further subjected to vertical automated injection molding machine for fabricating the tensile specimens and gear specimens to test the mechanical characteristics.

The various weight fractions of the acetal, graphene reinforced Teflon blend specimens were fabricated with the help of injection mold as per the ASTM standards.

2.3 Characterization

2.3.1 Spectral analysis

To discern any additional absorption bands that might have arisen during chemical modification, we employed Fourier transform infrared (FTIR) spectroscopy to examine both pure and surface-modified GNTs. For sample preparation, we meticulously blended 2 mg of GNTs with potassium bromide (KBr), resulting in a finely mixed compound. Subsequently, this compound was compacted into pellets and subjected to analysis using the Nicolet 6700 FTIR Spectrometer. Spectral data within the range of 4,000–700 cm^{-1} were acquired at a resolution of 2 cm^{-1}.

2.3.2 Mechanical properties

Prior to testing, all specimens were conditioned for 48 h at 50% (±5) relative humidity and 25°C.

2.3.3 Tensile properties

For the assessment of tensile characteristics, we adhered to the ASTM D 638-08 (Type I) standard test procedure, designed specifically for polymers. Tensile testing was conducted using the INSTRON 8801 universal testing equipment, equipped with a 100 kN load cell, a gauge length of 50 mm, and a crosshead speed set at 5 mm/min. Table 2 indicates multiple tests were performed, and the resulting mean values, along with standard deviations, were considered in the analysis.

2.3.4 Flexural properties

The flexural properties of the materials were assessed through a rigorous testing procedure conducted in strict accordance with the ASTM D 790 standard, utilizing the INSTRON 8801 universal testing machine. The test configuration involved a span length of 48 mm and a controlled cross head speed of 2 mm/min, with all tests conducted in the three-point bending mode. Fabricated samples were employed for this evaluation, and the resultant data included both mean values and standard deviations for each parameter.

Table 2: Composites identification and constituent composition

Specimen code	Acetal (%)	Teflon fiber	GNTs (%)	Functionalization
A	100		—	—
B	99.5		0.5	Purified
C	99.5		0.5	Carboxylation
D	99.5		0.5	Silanation
E	99.5		0.5	Carbonylation
F	99.5		0.5	Amination
G	99.75		0.25	Silanation
H	99		1	Silanation
I	98.5		1.5	Silanation
J	98		2	Silanation
K	95	5	—	
L	90	10	—	
M	85	15	—	
N	80	20	—	
O	94	5	1	
P	89	10	1	
Q	84	15	1	
R	79	20	1	

2.3.5 Wear test

To probe into the wear characteristics of the produced nanocomposites, comprehensive dry sliding wear tests were undertaken using a precision pin-on-disc apparatus, adhering closely to the guidelines set forth by ASTM D3702. For these tests, specimens were meticulously crafted from injection-molded flat test bars, each possessing dimensions of 3 × 3 × 25 mm^3, resulting in an abrasion area of 3 mm^2. The wear specimen pin was subjected to rotational motion against a flat steel disc measuring 180 mm in diameter and 10 mm in thickness.

During each test run, the initial surface roughness of the steel counterpart was maintained at a precise 0.25 µm. The tests were executed under various loads, specifically 15, 25, and 35 N, with a constant sliding velocity of 1 m/s. To monitor the dynamic frictional behavior, the frictional force was continuously monitored and meticulously recorded by the computer throughout the duration of each test. The

friction coefficient was calculated by dividing the applied load by the measured frictional force.

In preparation for each test iteration, both the specimens and the disc underwent thorough cleaning procedures to eliminate any contaminants that might interfere with the accuracy of the results. To determine the precise wear rate, measurements of the specimen's mass were acquired both before and after each test.

$$W_s = \Delta m/\rho \mathrm{Fn} L \ (\mathrm{mm}^3\ \mathrm{N}^{-1}\ \mathrm{m}^{-1}), \quad (1)$$

where Δm is the change in sample weight in g, ρ is the sample density in g mm^{-3}, Fn is the applied load in N, and L is the sliding distance in m. Three repetitive tests were conducted for each sample and the mean values of friction coefficient and specific wear rate were taken.

2.3.6 Morphological investigations

Within this research endeavor, an advanced Zeiss EVO 50 scanning electron microscope (SEM) serves as our primary tool for the comprehensive assessment of the morphological attributes of tension-fractured surfaces. Operating this SEM, we meticulously applied an acceleration voltage of 10 kV to ensure precise observations. To facilitate the SEM investigations, a crucial step involved the application of a gold ion-sputter coating to all our samples, rendering them conductive for the analytical processes.

Furthermore, for a more comprehensive examination of worn surfaces, we employed an Olympus optical microscope in conjunction with cutting-edge image analysis software. This combination of optical microscopy and digital analysis allowed us to delve into the intricacies of the surface morphology with exceptional clarity and precision. In addition to SEM and optical microscopy, we harnessed the capabilities of a cutting-edge TECNAI F 30 TEM to capture high-resolution TEM images of the composite materials. This multimodal approach to morphological analysis enabled us to gain a comprehensive understanding of the microstructure and surface characteristics of the specimens under scrutiny.

3 Results and discussion

3.1 FTIR process

To validate the surface changes in GNTs, FTIR spectroscopy was used to characterize all the treated and raw GNTs. The untreated and treated GNTs spectra in the band 4,000–400/cm are shown in Figure 7(a)–(e). The formation of C═O groups on the surface of GNTs in the process of carboxylation is observed in Figure 7(b) at the band 3,400/cm. Similarly, all the types of surface modifications are observed at different band zones under FTIR spectra. Furthermore, the –NH bonds that form as a result of the reaction of GNTs with EDA may be the cause of the tiny humps seen at 1,035 and 3,450/cm. A peak at 1,021/cm [16] can be seen in the spectra of silane-functionalized GNTs (Figure 7(e)), which can be attributed to the asymmetric stretching vibration of Si–O–Si bonds caused by the production of silaxane units during silanization of GNTs [17].

3.2 Tensile and flexural properties

Table 3 illustrates how GNT functionalization affects the tensile strength (TS) and modulus of Acetal/GNT composites. By comparing the pure acetal with 0.5 wt% of raw GNT reinforced acetal shows lower or reduced TS by 2.8% and shows increment in stiffness by 9%. With these results, it can be clearly visible that the surface medication of GNTs plays a vital role in the mechanical properties. In this context, GNTs with all the types of surface modifications (carboxylation, amination, and silanization) were considered to improve the mechanical properties of pure acetal and observed that the silanized GNTs showed better improvements in TS and modulus, by 23 and 38%, respectively, compared with all other surface modifications [18].

The surface modifications helped to remove the impurities on the surface of the GNTs resulting in improving the

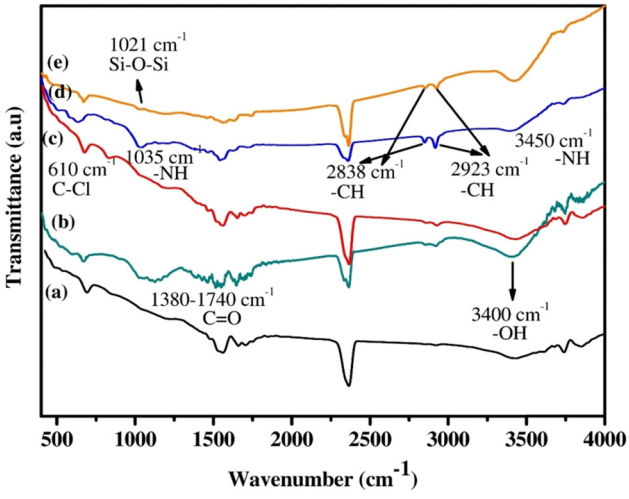

Figure 7: FTIR of (a) untreated GNTs, (b) C-GNTs, (c) T-GNTs, (d) A-GNTs, and (e) S-GNTs.

Table 3: Tensile and flexural values of all the tested specimens

Composite	TS	Tensile modulus (TM)	Flexural strength (FS)	Flexural modulus (FM)
A	49.5	1.7	82	2.5
B	46	1.8	83	2.6
C	55	2.25	100	3.2
D	60	2.4	110	3.5
E	55	2.2	101	3.3
F	57	2.3	108	3.4
G	51	1.8	90	2.8
H	65	2.5	120	3.7
I	62	2.5	115	3.7
J	55	2.5	110	3.8
K	48	1.65	62	2.75
L	41.8	1.6	60	2.7
M	45	1.45	50	2.4
N	38	1.4	45	2.3
O	63.5	2.5	115	3.6
P	63.6	2.6	110	3.75
Q	58	2.25	100	3.3
R	52	2	93	3.1

bonding strength of reinforcements and the matrix. The improved bonding strength led to improve the mechanical characteristics of the composite compared with pure GNTs and were observed clearly under SEM as shown in Figure 8(b)–(e). Further, detailed observation are carried out for all the surface modifications of GNTs under SEM and pullouts are rarely identified in the silanized GNT composites.

As discussed earlier, the dispersion rate of GNTs in the matrix and bonding strength purely depends on the surface modifications. From Figure 8, it is clearly observed that the (composite B) specimen dispersion rate is poor resulting in decrease in the strength compared to the neat acetal. The uniform dispersion and bonding strength of the silanized-treated composites are clearly observed in Figure 8(g) than the other types of surface modifications helps to improve the tensile and flexural strength (FS) by 3% compared to pure acetal. The addition of silanized treated GNTs in the acetal improves the mechanical characteristics up to 1 wt% as shown in Table 3 and shows a decrement in the strength even after addition of GNTs due to its agglomeration. However, the silanized treated 1 wt% GNTs with acetal increased its TS, TM, FS, and FM by 34, 46, 43, and 48%, respectively.

3.3 Fatigue results

To evaluate the impact of incorporating a lubricating additive and reinforcing acetal with 1 wt% silanized GNTs on fatigue behavior, tension-tension fatigue tests were conducted on four composite variants: A (pure acetal), L (10% Teflon), H (1 wt% silanized GNTs), and P (10% Teflon + 1 wt% silanized GNTs). The experimental parameters for the fatigue tests are summarized in Table 4. The fatigue life data were analyzed and modeled using the power law approach [19].

$$\sigma_{\max} = AN_{\mathrm{f}}^{B}. \tag{2}$$

In this study, A represents the fatigue strength coefficient, and B denotes the fatigue strength exponent. The addition of Teflon adversely impacted the fatigue strength compared to pure acetal. This decline is likely due to the agglomeration of Teflon microparticles, which create local stress concentrations. The effect of reinforcing acetal and acetal/Teflon composites with 1 wt% silane-functionalized GNTs on fatigue strength is evident from the S–N curves for composites H and P.

Incorporating functionalized GNTs into acetal significantly improved fatigue strength, attributed to uniform dispersion and strong interfacial bonding between the GNTs and the matrix. Similarly, hybrid composites containing 1 wt% silanized GNTs and 10 wt% Teflon demonstrated better fatigue strength than neat acetal and composite L. However, their performance was slightly inferior to composite H, suggesting that the synergy of GNTs and Teflon improves fatigue properties but not to the extent of GNTs alone as observed in Figure 9.

3.4 Wear

The fabricated composites were subjected to dry sliding wear tests under three distinct loads. The influence of treated GNTs with acetal on wear rate and frictional coefficient [19] is shown in Figures 10 and 11. The specific wear rate of a specimen always depends on the applied load and if the load increases, then the frictional coefficient decreases [20,21]. The worn surface of the specimen under 15 and 35 N loads are shown in Figure 12a and b. The deep grooves on the surface of the specimen are formed at 35 N and opposed to form shallow grooves on the surface at 15 N. When the fabricated material are used for gear applications, the gears are commonly subjected to continuous engage and disengage known as bending stresses, due to which maximum wear rate takes place under heavy loads [22,23].

However, in composite B (0.5 wt% R-GNTs), the specific wear rate increases by 9 and 6% by imposing the loads at 15 and 25, and further increases at 35 N. The specific wear rate of composite B increases due to its weak bonding strength between the matrix and fiber. Due to the presence of impurities on the surface of raw GNTs, the possibility of bonding strength is low and which causes increment in the wear

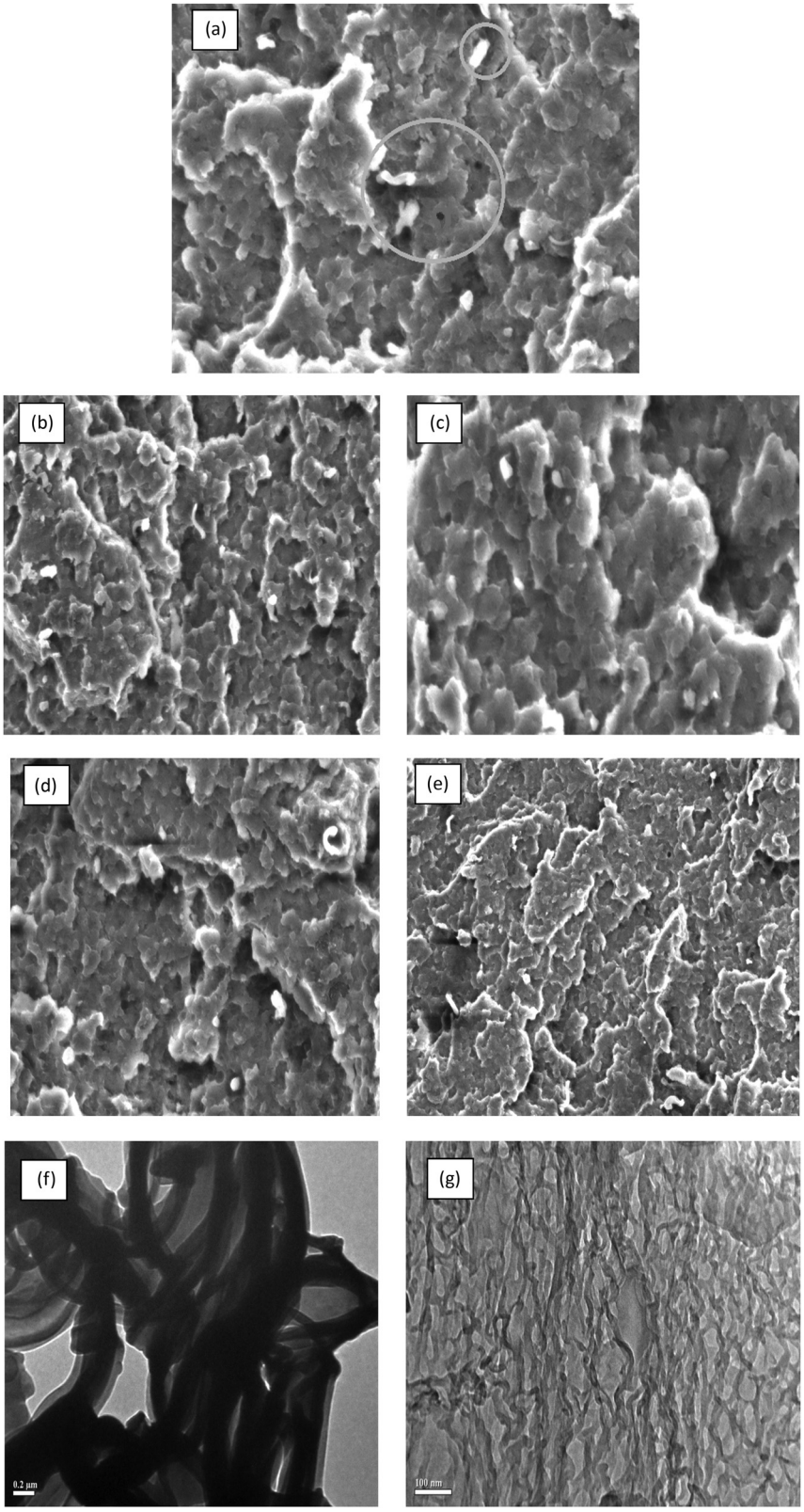

Figure 8: SEM images of tensile fractured surfaces of composites: (a) A (100% acetal), (b) B (acetal with untreated GNT), (c) C (acetal with C-GNT), (d) D (acetal with S-GNT), and (e) E (acetal with T-GNT), and TEM images of composites: (f) B (acetal with untreated GNT) and (g) D (acetal with S-GNT).

Table 4: Solutions obtained for acetal/GNTs composite specimens

Loss function method	Solution
LFA – 1	H > P > I > O > J > D > F > Q > E > C > R > G > B > A > K > L > M > N
LFA – 2	H > P > I > O > J > D > F > Q > E > C > R > G > B > A > K > L > M > N
LFA – 3	H > P > I > O > J > D > F > Q > E > C > R > G > B > A > K > L > M > N

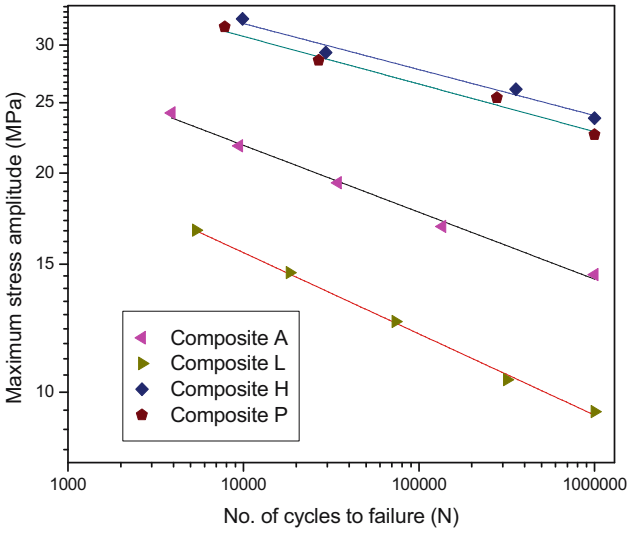

Figure 9: Fatigue life of acetal/Teflon and acetal/Teflon/GNT composites.

rate. The addition of raw GNTs beyond the 1 wt% forms agglomeration in the structure, due to this, the excess material will form as a third body and can be separated easily from the composite and finally it leads to increase in the wear rate drastically.

The addition of silane-treated GNTs in acetal increases the wear resistance and decreases the coefficient of friction at the considered loads. The wear characteristics of S-GNTs are good due to its interfacial bonding strength and improves the strength, toughness, and stiffness [24,25] under all the considered loads. The obtained results of S-GNTs for specific wear rate and coefficient of friction is quite good when compared to the other surface modification methods of GNTs. Due to increment in the mechanical properties and wear characteristics of S-GNTs, the smooth worn surfaces are formed on the material compared with pure acetal, and the raw GNTs shown in Figure 12.

The impact of GNTs in acetal under specific wear rate and coefficient of friction are shown in Figures 13 and 14. The wear rate of the composite decreases with the addition of GNTs up to 1 wt% and increases the wear rate beyond the addition due to its agglomeration in the structure and 1 wt% is considered as an optimum composition of the GNTs in the acetal. The coefficient of friction is decreasing with the addition of GNTs and less shallow grooves are formed on the surface of the S-GNTs compared with composite H and composite D as shown in Figure 13.

3.5 Loss function approach

The loss function approach [26] is a simple, compelling, and straightforward strategy for choosing the best ideal

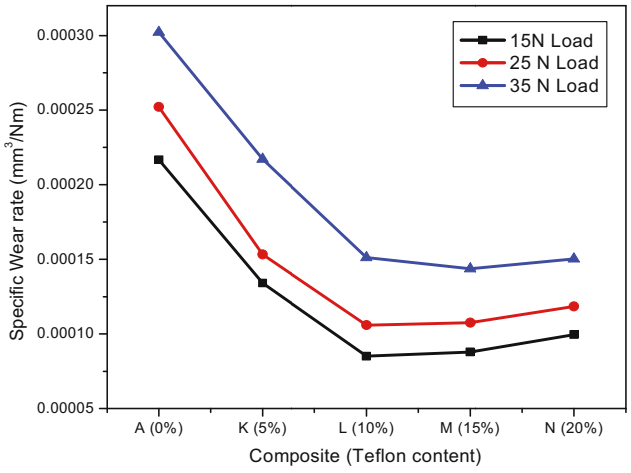

Figure 10: Specific wear rate of acetal/Teflon fiber composite.

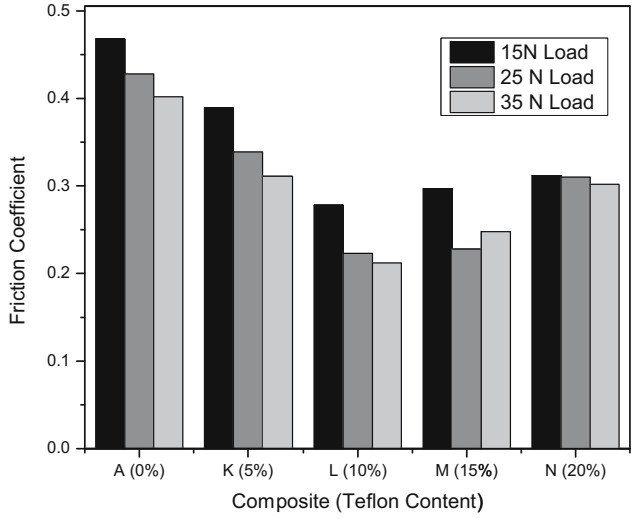

Figure 11: Friction coefficient of acetal/Teflon composites.

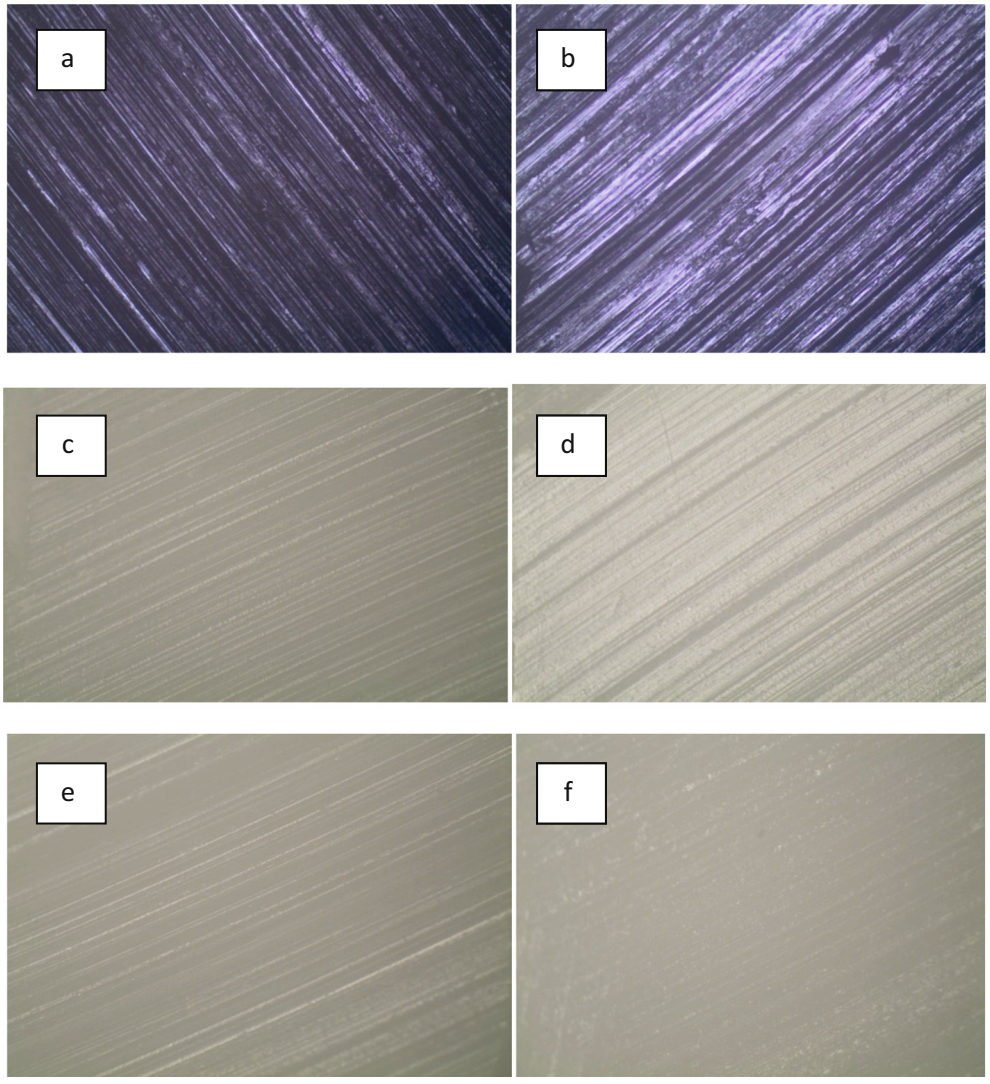

Figure 12: Worn surfaces of (a) composite A (at 15 N load), (b) composite A at 35 N load, (c) composite L, (d) composite M, (e) composite H, and (f) composite P.

solution for decision makers. By using this technique, we will get the ideal best choice among the available options. The loss for choosing each alternative is calculated relative to the ideal best alternative. However, attributes are classified as beneficiaries and non-beneficiaries. Higher values are preferred for beneficiary attributes and lower values are preferred for non-beneficiary attributes [27,28]. In general, no alternative has all high-value beneficiary attributes and all low-value non-beneficiary attributes. Some choices may have the best values for some attributes and higher levels for other less desirable values. Attributes also have different weights from each other [29]. These conflicting nature forces decision makers to choose the best option based on several criteria. Similar to the TOPSIS method [30], the Euclidean distance of alternatives is used to select the best alternative from the ideal best alternative and the ideal worst alternative. In this method of loss function approach, the ideal best choice consists of all high values of beneficiary attributes and low values of non-beneficiary attributes. Losses are calculated using linear, quadratic, and cubic loss functions.

Total loss caused by alternative using linear loss function is calculated as

$$L_{\mathrm{f}} = \sum_{J \in s} . \{\mathrm{W_s}(x_{\mathrm{fj}} - x_{\min})/(x_{\max} - x_{\min})\} + \sum_{J \in H} . \{\mathrm{W_H}(x_{\max} - x_{\mathrm{fj}})/(x_{\max} - x_{\min})\}, \tag{3}$$

where W_{S} is the weight of the non-beneficiary and W_{H} is the weight of the beneficiary attributes.

Total loss caused by alternative using quadratic loss function is calculated as

$$L_f = \sum_{J\epsilon s} . \{W_s(x_{fj} - x_{min})^2 / (x_{max} - x_{min})^2\} + \sum_{J\epsilon H} . \{W_H(x_{max} - x_{fj})^2 / (x_{max} - x_{min})^2\}. \quad (4)$$

Total loss caused by alternative using cubic loss function is calculated as

$$L_f = \sum_{J\epsilon s} . \{W_s(x_{fj} - x_{min})^3 / (x_{max} - x_{min})^3\} + \sum_{J\epsilon H} . \{W_H(x_{max} - x_{fj})^3 / (x_{max} - x_{min})^3\}. \quad (5)$$

In general process, the total loss occurred by the alternative f can be observed as

$$L_f = \sum_{J\epsilon s} . \{W_s(x_{fj} - x_{min})^n / (x_{max} - x_{min})^n\} + \sum_{J\epsilon H} . \{W_H(x_{max} - x_{fj})^n / (x_{max} - x_{min})^n\}, \quad (6)$$

where n is the loss function index, and $n = 1, 2$, and 3 for the linear, quadratic, and cubic functions, respectively. The loss function index in the loss function approach is mentioned as LFA – n.

Implementation of loss function approach:

The general steps involved in the loss function to solve any problem is given as

- Step 1: Obtain the data pertaining to all available alternatives. The alternatives have to convert to quantitative nature.
- Step 2: The weight of each attribute has to be determined using any of the existing methods.
- Step 3: Assigning the maximum loss for each attribute equal to the weight of the respective attribute.
- Step 4: The proper loss functions to be used for each attribute are to be decided. The loss function approaches are linear, quadratic, and cubic functions.
- Step 5: Compute the loss of choosing an alternative using Eqs. (2)–(5). Now arrange the alternatives in the ascending order of their loss values, which obtains the preference order of each alternative.

From the data (Table 3), four attributes, namely, TS, TM, FS, and FM, with 18 acetal/GNTs composite specimens as alternatives are taken into consideration for identifying the ideal best solution for the material selection problem by adopting the loss function approach.

Computing the solution using linear, quadratic, and cubic loss functions

1. The data of the alternatives is mentioned in Table 3. The first column of Table 3 represents various alternatives of composite specimens from 1 to 18.
2. The four attributes such as TS, TM, FS, and FM are considered as quantitative.
3. The weights of four attributes are calculated by using AHP entropy method (Al-Aomar, 2010).

   $W_1 = 0.1379$; $W_2 = 0.2458$; $W_3 = 0.4502$; $W_4 = 0.1658$.
4. Now the material selection problem is solved using linear, quadratic, and cubic loss functions.

Initially considering the linear loss function, from Table 4, the prominent data are obtained as

$X^1_{max} = 65$; $X^2_{max} = 2.6$; $X^3_{max} = 120$; $X^4_{max} = 3.8$.

$X^1_{min} = 38$; $X^2_{min} = 1.4$; $X^3_{min} = 45$; $X^4_{min} = 2.3$.

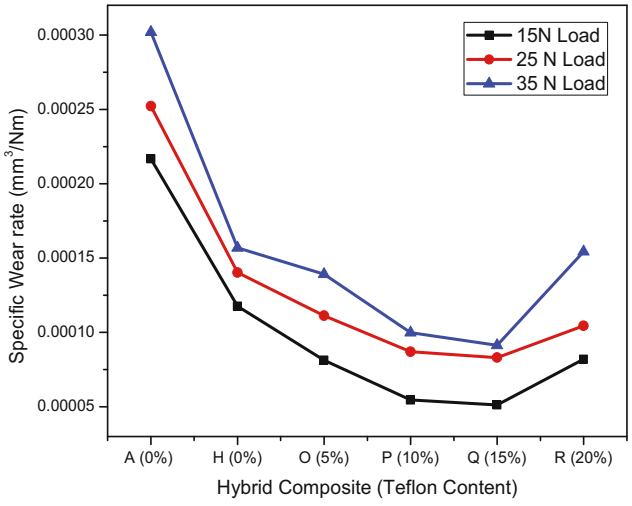

Figure 13: Specific wear rate of acetal/Teflon/GNT composite with 1 wt% GNTs and varying Teflon content.

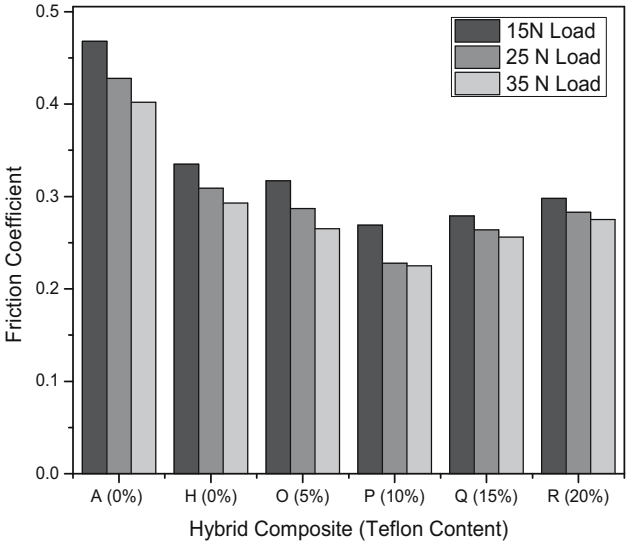

Figure 14: Friction coefficient of acetal/Teflon/GNT composite with 1 wt% GNTs and varying Teflon content.

Finally, the losses for choosing various alternatives are computed using Eq. (2) in the respective losses are shown below:

L_A = 0.364487; L_B = 0.384153; L_C = 0.690762; L_D = 0.840258; L_E = 0.697577; L_F = 0.781371; L_G = 0.473844; L_H = 0.968451; L_I = 0.923102; L_J = 0.86837; L_K = 0.25415; L_L = 0.194684; L_M = 0.087094; L_N = 0; L_O = 0.919711; L_P = 0.927282; L_Q = 0.71715; L_R = 0.57112.

The material selection solution using linear loss function is observed as

H > P > I > O > J > D > F > Q > E > C > R > G > B > A > K > L > M > N

Using quadratic loss functions, the losses for choosing various alternatives are computed using Eq. (2) and the respective losses are shown below:

L_A = 0.152932; L_B = 0.161656; L_C = 0.479925; L_D = 0.706717; L_E = 0.488729; L_F = 0.613545; L_G = 0.239832; L_H = 0.939347; L_I = 0.852354; L_J = 0.589278; L_K = 0.067661; L_L = 0.039369; L_M = 0.01244; L_N = 0; L_O = 0.846505; L_P = 0.863124; L_Q = 0.514941; L_R = 0.330177.

The material selection solution using quadratic loss function is observed as

H > P > I > O > J > D > F > Q > E > C > R > G > B > A > K > L > M > N.

Using cubic loss functions the losses for choosing various alternatives are computed using Eq. (3) in the respective losses are shown below:

L_A = 0.068958; L_B = 0.072587; L_C = 0.335227; L_D = 0.594969; L_E = 0.343875; L_F = 0.484102; L_G = 0.127908; L_H = 0.912496; L_I = 0.787242; L_J = 0.682808; L_K = 0.018956; L_L = 0.00827; L_M = 0.002605; L_N = 0; L_O = 0.779689; L_P = 0.806433; L_Q = 0.370186; L_R = 0.193168.

The material selection solution using cubic loss function is observed as

H > P > I > O > J > D > F > Q > E > C > R > G > B > A > K > L > M > N.

The observations drawn from Table 4 indicates the better performance of composite H (99 wt% acetal and 1 wt% silanized GNTs) when compared to the other compositions in static conditions. It is also observed that the composite H specimen is the best alternative choice among the given set of attributes using loss functions approach.

4 Conclusion

This study demonstrates the significant benefits of functionalizing GNTs and optimizing fiber weight fractions in acetal composites. The results show that silanized GNTs enhance mechanical strength, wear resistance, and reduce friction, outperforming other surface-modified GNTs. Additionally, incorporating 10 wt% Teflon fibers further increases wear resistance and bending strength. The optimal combination of 1 wt% silanized GNTs and 10 wt% Teflon fiber creates a composite superior to neat acetal, offering increased strength, stiffness, and durability. This makes the composite ideal for high-load applications such as acetal gears, where enhanced performance and longevity are critical.

5 Future study recommendations

Future research should focus on exploring additional functionalization techniques, refining fiber dispersion methods, and evaluating long-term performance under varying environmental conditions. Additionally, comparisons with commercial acetal and conventional plastics are necessary to confirm the composite's superiority in real-world applications.

Acknowledgments: The authors express their gratitude to the Department of Mechanical Engineering at Andhra University for providing the laboratory facilities essential for our research. We also extend our heartfelt thanks to GITAM Deemed to be University, Visakhapatnam, for granting us access to their testing facilities.

Funding information: Authors state no funding involved.

Author contributions: Vijaya Babu Vommi: basic study design, literature review, and resources. Chaitanya Mayee Makkuva: data collection, materials fabrication, and mechanical properties analysis. All authors have accepted responsibility for the entire content of this manuscript and approved its submission.

Conflict of interest: Authors state no conflict of interest.

Data availability statement: All data generated or analyzed during this study are included in this published article.

References

[1] Smith J, Brown K. Polymer gears in industry: applications and properties. J Ind Mater Eng. 2015;45(3):101–10.
[2] Gupta A, Wang Y. Abrasion and wear resistance of acetal polymers in mechanical applications. Wear. 2017;386–387:1–6.
[3] Lee H, Kim S. Fatigue resistance of acetal gears under load-bearing conditions. Polym Sci Today. 2018;34(2):213–9.

[4] Thompson L, Zhang T. Advancements in reinforcing acetal polymers for high- performance applications. Compos Mater. 2019;29(5):325–33.
[5] Chandra R, Patel V. Thermal properties and wear mechanisms in polymer gears. Int J Mech Eng. 2020;54(7):645–54.
[6] Garcia M, Lin P. Lubrication strategies in polymer composites: effects on gear life. Tribol Int. 2021;153:106667.
[7] Patel D, Sharma N. Enhancement of acetal gears through nano-reinforcements. Mater Sci Adv. 2022;48(9):871–80.
[8] Wang R, Zhao Q. Graphene nanotube functionalization for improved polymer composites. Nano Mater Eng. 2023;12(4):123–34.
[9] Pötschke P, Villmow T, Krause B, Kretzschmar B. Influence of twin screw extrusion conditions on MWCNT length and dispersion and resulting electrical and mechanical properties of polycarbonate composites. Polymers. 2024;16(19):2694. doi: 10.3390/polym16192694.
[10] Mathur RB, Pande S, Singh BP, Dhami TL. Electrical and mechanical properties of multi-walled carbon nanotubes reinforced PMMA and PS composites. Polym Compos. 2008;29(7):717–27.
[11] Goriparthi BK, Naveen PNE, Ravi Sankar H, Ghosh S. Effect of functionalization and concentration of carbon nanotubes on mechanical, wear and fatigue behaviours of polyoxymethylene/carbon nanotube nanocomposites. Bull Mater Sci. Jun 2019;42(3):98. doi: 10.1007/s12034-019-1746-z.
[12] Goriparthi BK, Naga Eswar Naveen P, Ravi Sankar H. Performance evaluation of composite gears composed of POM, CNTs, and PTFE. Polym Compos. Mar 2021;42(3):1123–34. doi: 10.1002/pc.25887.
[13] Shivakumar H. The reinforcing effect of graphene on the mechanical properties of carbon-epoxy composites. Open J Compos Mater. 2020;10:27–44.
[14] Ramanjaneyulu S. Design and development of graphene reinforced acetal copolymer plastic gears and its performance evaluation. Mater Today: Proc. 2017;4:8678–87.
[15] Naveen PNE, Prasad RV, Rajendra D. Experimental testing and evaluation of coconut coir/rice husk fiber reinforced with polymer composites. In: Pujari S, Srikiran S, Subramonian S, editors. Recent Advances in Material Sciences. Lecture Notes on Multidisciplinary Industrial Engineering. Singapore: Springer; 2019. p. 209–15, doi: 10.1007/978-981-13-7643-6_17.
[16] Shen MY, Chang TY, Hsieh TH, Li YL, Chiang CL, Yang H, et al. Mechanical properties and tensile fatigue of graphene nanoplatelets reinforced polymer nanocomposites. J Nanomater. 2013;2013:565401. doi: 10.1155/2013/565401.
[17] Eayal Awwad KY, Yousif BF, Fallahnezhad K, Saleh K, Zeng X. Influence of graphene nanoplatelets on mechanical properties and adhesive wear performance of epoxy-based composites. Friction. 2021;9(4):856–75. doi: 10.1007/s40544-020-0453-5.
[18] Kumar S, Saha A. Graphene nanoplatelets/organic wood dust hybrid composites: physical, mechanical and thermal characterization. Iran. Polym. J. 2021;30(9): 935–51. doi: 10.1007/s13726-021-00946-5.
[19] Srinath G, Gnanamoorthy R. Effect of short fibre reinforcement on the friction and wear behaviour of nylon 66. Appl Compos Mater. Nov 2005;12(6):369–83. doi: 10.1007/s10443-005-5824-6.
[20] Tunalioglu MS, Agca BV. Wear and service life of 3-D printed polymeric gears. Polymers. 2022;14(10):2064. doi: 10.3390/polym14102064.
[21] Polanec B, Zupanič F, Bončina T, Tašner F, Glodež S. Experimental investigation of the wear behaviour of coated polymer gears. Polymers. 2021;13(20):3588. doi: 10.3390/polym13203588.
[22] Lundvall O, Strömberg N, Klarbring A. A flexible multi-body approach for frictional contact in spur gears. J Sound Vib. 2004;278(3):479–99. doi: 10.1016/j.jsv.2003.10.057.
[23] Juarbe FM, Hanley MA. Factors affecting fatigue strength of nylon gears. J Mech Des. 1981;103(2):543–8.
[24] Shahil KMF, Balandin AA. Graphene-multilayer graphene nanocomposites as highly efficient thermal interface materials. Nano Lett. Feb 2012;12(2):861–67. doi: 10.1021/nl203906r.
[25] Cui T, Mukherjee S, Sudeep PM, Colas G, Najafi F, Tam J, et al. Fatigue of graphene. Nat Mater. 2020;19(4):405–11. doi: 10.1038/s41563-019-0586-y.
[26] Vommi VB, Kakollu SR. A simple approach to multiple attribute decision making using loss functions. J Ind Eng Int. Mar 2017;13(1):107–16. doi: 10.1007/s40092-016-0174-6.
[27] González-Prida V, Barberá L, Viveros P, Crespo A. Dynamic analytic hierarchy process: AHP method adapted to a changing environment. In IFAC Proceedings Volumes (IFAC-PapersOnline). IFAC Secretariat; 2012. p. 25–9. doi: 10.3182/20121122-2-ES-4026.00005.
[28] Łatuszyńska A. Multiple-criteria decision analysis using TOPSIS method for interval data in research into the level of information society development. Folia Oeconomica Stetin. Jul 2014;13(2):63–76. doi: 10.2478/foli-2013-0015.
[29] Al-Aomar R. A combined AHP-entropy method for deriving subjective and objective criteria weights. Int J Ind Eng. 2010;17(1):12–24.
[30] Pavić Z, Novoselac V. Notes on TOPSIS method. Int J Eng Res. 2013;1:5–12.